nano energy
Editor-in-Chief: Zhong Lin Wang

RAPID COMMUNICATION

Doped hole transport layer for efficiency enhancement in planar heterojunction organolead trihalide perovskite solar cells

CrossMark

Qi Wang, Cheng Bi, Jinsong Huang*

Department of Mechanical and Materials Engineering, University of Nebraska-Lincoln, Lincoln, NE 68588, USA

Abstract
We demonstrated the efficiency of a solution-processed planar heterojunction organometallic trihalide perovskite solar cell can be increased to 17.5% through doping the hole transporting layer for reducing the resistivity. Doped Poly(triaryl amine) (PTAA) by 2,3,5,6-Tetrafluoro-7,7,8,8-Tetracyanoquinodimethane (F4-TCNQ) reduced device series resistance by three-folds, increasing the device fill factor to 74%, open circuit voltage to 1.09 V without sacrificing the short circuit current. This study reveals that the high resistivity of currently broadly applied polymer hole transport layer limits the device efficiency, and points a new direction to improve the device efficiency.
© 2015 Elsevier Ltd. All rights reserved.

Introduction

In the past five years, organometallic trihalide perovskite (OTP) solar cells have been attracting tremendous interest because of their unique properties for photovoltaic applications, such as strong absorption in the visible spectrum [1], long and balanced carrier diffusion length [2-5], solution processability and insensitivity to defect formation [6,7]. Recently, a number of endeavors have been directed to developing charge transport materials to further increase the efficiency of OTP

photovoltaic devices [8-12]. While a lot of new hole transport materials (HTMs) have been synthesized and applied in the inverted structure OTP devices where HTMs were spun directly on top of the perovskite films [8,9,11], most of these HTMs are difficult to be applied in regular structure planar heterojunction (PHJ) OTP devices with the hole transport layer (HTL) underneath the perovskite layer. This is because the general solvents used for the OTP, such as N,N-dimethylformamide (DMF) and dimethyl sulfoxide (DMSO), have too good solubility and can wash off most commonly used small molecular HTMs, such as 2,2′,7,7′-Tetrakis-(N,N-di-4-methoxyphenylamino)-9,9′-spirobifluorene (Spiro-OMeTAD). Therefore, although solution processed regular structure PHJ OTP solar cells have shown higher fill factor (*FF*) of over than 80% and great promise to

*Corresponding author.
  E-mail address: jhuang2@unl.edu (J. Huang).

achieve higher power conversion efficiency (PCE), most of these PHJ OTP devices still adopted Poly(3,4-ethylenedioxythiophene) Polystyrene sulfonate (PEDOT:PSS) as HTL [13-15]. However, the low work function of PEDOT:PSS caused a relatively small open circuit voltage (V_{OC}) of around 0.90 V in these PHJ devices, compared to the typical V_{OC} of >1.05 V in the inverted structure OTP devices.[14,16-18] Recently, polymer HTMs have been studied because of its sustainability to DMF wash, for example, poly[N, N′-bis(4-butylphenyl)-N, N′-bis(phenyl)benzidine] (poly-TPD), was introduced into PHJ perovskite devices with device V_{OC} greatly increased to 1.10 V. [19,20] Meanwhile, we found that another polymer HTM, Poly (triaryl amine) (PTAA), also showed great capability to increase device V_{OC} and survive the DMF wash. However, the PCE of these polymer HTLs based OTP devices was still around 15% [19,20]. Compared with the best reported efficiency of PEDOT:PSS based perovskite devices, the higher V_{OC} of polymer HTL based OPT devices was obtained at the expense of a smaller fill factor (FF) [13,14,16]. We speculate that the higher resistivity of these polymer HTMs than PEDOT:PSS may hinder charge extraction efficiency which reduces FF of these devices. Here, we report highly efficient solution-processed PHJ perovskite solar cells using 2,3,5,6-Tetrafluoro-7,7,8,8-tetracyanoquinodimethane (F4-TCNQ) doped PTAA as the HTL. F4-TCNQ doping was found to reduce the series resistance of the PTAA device by three times, which improved the device PCE, especially when thick HTL was used.

Experimental section

Device fabrication and characterization

The methods of cleaning ITO glass, methylammonium iodide (MAI) synthesis can be found elsewhere [13]. The PTAA and F4-TCNQ were dissolved in toluene and mixed by desired F4-TCNQ/PTAA ratios ranging from 0.01 wt% to 10 wt%. The mixture was stirred and heated at 70 °C overnight. Device with highest PCE was made by 10 mg/ml doped PTAA solution under a spin speed of 4000 RPM. For the device fabrication, small amount (∼10 wt%) of 4,4′,4″-Tris[phenyl (m-tolyl)amino]triphenylamine (m-MTDATA) was mixed in the PTAA solution because the bare PTAA film was so smooth and non-wetting to DMF that PbI_2 precursor was hardly spun on top of it. The perovskite films for device fabrication were made by interdiffusion method, in which PbI_2 and MAI were sequentially spun on the substrates. The concentration of PbI_2 was fixed at the 600 mg/ml and the concentration of MAI was varied from 50 mg/ml to 70 mg/ml. Before depositing MAI, the spun PbI_2 films were annealed at 80-100 °C to remove DMF. The spun perovskite films were annealed at 100 °C on hotplate under the cover of a glass petri dish. 10-30 μL of DMF solvent was added at the edge of the petri dish during annealing process. After that, [6,6]-phenyl-C61-butyric acid methyl ester (PCBM) (dissolved in DCB, 2 wt%) was spin coated on top of the perovskite layer at 6000 RPM for 35 s. The films were annealed at 100 °C for 60 min. Then 20 nm thickness of C_{60} was thermally evaporated with a deposition rate of 0.5 Å/s. The devices were finished by the evaporation of 7 nm 2,9-dimethyl-4,7-diphenyl-1,10-phenanthroline (BCP) and 100 nm thick aluminum electrode.

Generally, the procedures for making PTAA films in the resistivity measurement were same with that for device fabrication. But thicker PTAA layer of 200 nm was used for increasing the signal-noise ratio. The schematic diagram of setup and the method of measuring resistivity can be found elsewhere [21]. The four probe measurement was conducted at atmosphere without encapsulation. Film thickness was measured by Bruker Dektak XTL step profiler. The photocurrents of the devices were measured under AM 1.5 G irradiation (100 mW cm^{-2}) with an xenon-lamp-based solar simulator (Oriel 67005, 150 W Solar Simulator). A Schott visible-colour glass-filtered (KG5 colour-filtered) Si diode (Hamamatsu S1133) was used to calibrate the light intensity before photocurrent measurement. Keithley 2400 Source-Meter was used for recording the I-V measurement.

Fill factor calculation

The method of calculating FF was based on assumption that the maximum power output of the solar cell approximately equals to the power in the absence of series resistance minus the power lose of the series resistance.[22]

$$FF = FF' * (1 - r) \tag{1}$$

where FF and FF′ are the fill factor of devices with and without series resistance, respectively. r and ideal fill factor FF′ can be described by the following equations [22]:

$$r = \frac{R_s}{R'} \tag{2}$$

$$R' = \frac{V_{MP}}{I_{MP}} \tag{3}$$

$$I_{MP} = I_L - I_0 \exp \frac{q V_{MP}}{nkT} \tag{4}$$

where R_S is the series resistance. I_{MP} and V_{MP} are the maximum-power-point current and voltage of the device with negligible series resistance and infinitely large shunt resistance. I_L is light generated photocurrent, I_0 is dark saturation current, q is elemental charge, n is ideal factor, k is Boltzmann constant, T is temperature. Here, we assumed dark saturation current equals to $1*10^{-16}$ mA/cm^2. Series resistance can be calculated based on resistivity measured by four probe method and the device geometry. Assuming n equals to 1, I_L equals to 24 mA/cm^2 based on the integrated sunlight spectrum of radiance, the device FFs can be calculated by Eq. (1).

Result and discussion

Figure 1a shows the structure of the devices in this study. The perovskite films were made by interdiffusion method, where lead iodide (PbI_2) and methylammonium iodide (MAI) were sequentially spun onto the substrates, followed by a thermal annealing driven diffusion process [14]. It was discovered by us the surface of $MAPbI_3$ can decompose during the thermal annealing process even though the annealing temperature was as low as 110 °C. MAI was found to evaporate from the film surface, leaving Pb^{2+} rich surface, as revealed by the composition sensitive scanning probe microscopy technique [23]. Our density function
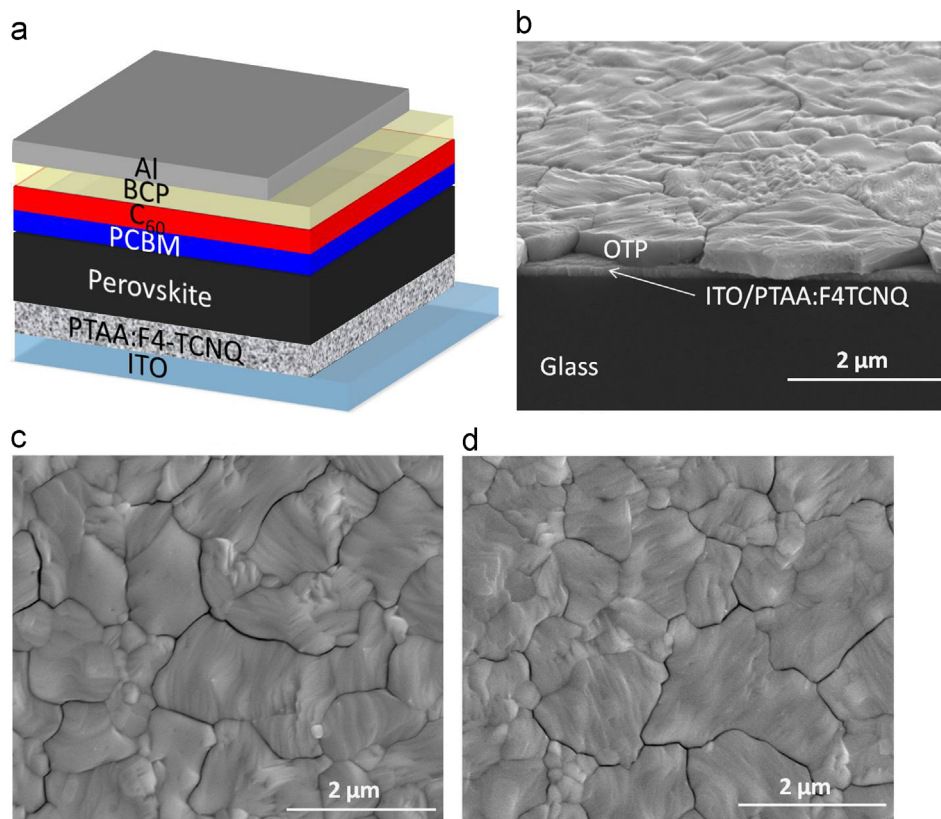
Figure 1 (a) Schematic structure of the devices in this study. The thickness of each layer was not in scale with the real thickness for clarity. (b) Cross-section scanning electron microscopy picture of perovskite on 1 wt% F4-TCNQ doped PTAA layer. SEM images of perovskite films on non-doped PTAA (c) and 1 wt% F4-TCNQ doped PTAA (d).

theory calculation showed that the Pb^{2+} clusters cause deep electron and hole traps on the perovskite surface [23]. Double-layer fullerenes were used as electron transport layer, which can effectively passivate the charge traps on top of the perovskite film surface generated by the surface decomposition during thermal annealing [14,16,23]. High concentration of perovskite precursors was used in this study for stronger absorption. In addition, solvent annealing was applied in this study for larger grain size [16]. Details about device fabrication and measurements could be found in the experimental section. Figure 1b shows the cross-section scanning electron microscopy (SEM) of perovskite films on doped PTAA substrates. It is noted that the grain size of perovskite on PTAA substrates is much larger than that on PEDOT:PSS substrates.[14,24] The non-wetting surface of PTAA is beneficial for grain growth because of lower nucleus density and less dragging force [25]. The larger grain size of several micrometers observed on the PTAA substrates are of importance in suppressing grain boundary traps to obtain better device efficiency. Figure 1c and d shows the SEM images of perovskite on non-doped PTAA and 1 wt% F4-TCNQ doped PTAA film, respectively. The morphology did not exhibit noticeable difference before and after doping, excluding the influence of dopant on perovskite morphology.

Figure 2a shows the current density–voltage (*J-V*) curves of devices with different F4-TCNQ doping concentration in the HTLs. The thickness of the HTL was kept unchanged by using a same solution concentration and spin rate. The changed doping level was found to have a significant impact on device performance, especially *FF*. As shown in the Figure 2b, the devices with 20 nm non-doped PTAA layer exhibited a low *FF* of 65%. After doping the PTAA layer by 1 wt% F4-TCNQ, the device *FF* was increased to 74%. Further increasing doping level to 10 wt% deteriorated device PCE by reducing *FF* to 64%. The device with 1 wt% F4-TCNQ doped PTAA showed the highest efficiency with a J_{SC} of 21.6 mA/cm², a V_{OC} of 1.09 V, a *FF* of 74% and PCE of 17.5% under 1 sun illumination. Corresponding data can be found in Table 1. Figure 2c–d shows the external quantum efficiency (EQE), steady photocurrent output and stabilized PCE of the device with 1 wt% F4-TCNQ dopant in the HTL. The calculated J_{SC} of 21.0 mA/cm² from EQE is in good agreement with that from *J-V* measurement. And the steady photocurrent measured at the maximum power point (0.85 V) is the same with that measured from *J-V* scanning, excluding the existence of obvious photocurrent hysteresis in our PHJ devices. The stabilized efficiency is 17.5%, confirming the accuracy of our device efficiency characterization. The absence of photocurrent hysteresis can be explained by the large grain grown on PTAA, and the application of double fullerene layer on the devices, which effectively reduce charge trap density at grain boundaries and film surface [13,26].

The *FF* enhancement can be explained by the series resistance reduction of the PTAA HTL caused by F4-TCNQ doping. To verify this, the series resistance of devices with different F4-TCNQ doping concentrations was derived by the
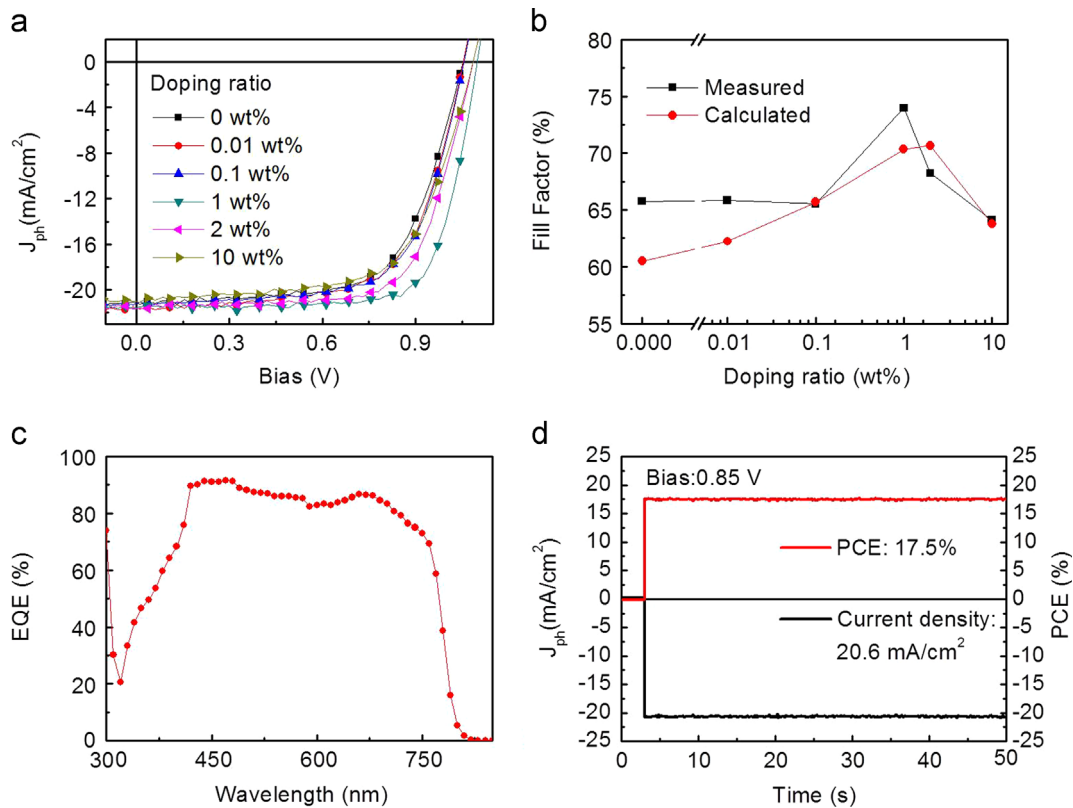
Figure 2 (a) The photocurrents of the devices under AM 1.5 simulated illumination with different doping levels of PTAA layer. (b) Calculated and experimental fill factors of devices with different doping levels of HTL. External quantum efficiency (c) and steady maximum power output measurement (d) of the best device.

Table 1 Perovskite device performance with different F4-TCNQ doping levels in PTAA layers. R_S is device series resistances derived from I-V curves and R_S' is series resistances of PTAA films derived from a four-probe method.

Doping ratio (wt%)	J_{SC} (mA/cm²)	V_{OC} (V)	FF (%)	PCE (%)	R_S (Ω cm²)	R_S' (Ω cm²)
0	21.6	1.05	65.7	14.8	9.07	12.9
0.01	21.0	1.05	65.8	14.5	7.57	12.1
0.1	21.5	1.05	65.5	14.8	7.72	10.6
1	21.6	1.09	74.0	17.5	6.07	8.4
2	21.0	1.09	68.2	15.6	8.56	8.2
10	21.2	1.09	64.1	14.8	9.77	11.4

slope of J-V curves. As shown in Figure 3, doping the PTAA film by 1 wt% F4-TCNQ reduced the device series resistance from 9.07 Ω cm² for non-doped PTAA to 6.07 Ω cm². Further increasing F4-TCNQ doping level to 10 wt% increased the device series resistance to 9.77 Ω cm², most likely caused by the increased aggregation of F4-TCNQ [27-30]. The series resistance derived from the J-V curve slope can be an indirect evidence for the doping effect because it represents the series resistance of the whole device rather than the PTAA films. To confirm the doping effect of F4-TCNQ, we further conducted four-probe measurements on the PTAA films with different doping levels. Details about four probe measurement can be found in the experimental section and our previous publication [21]. It should be noted that

200 nm PTAA film, which is much thicker than the PTAA layer in devices, was used to reduce noise in the four-probe measurement. To estimate the series resistance of the PTAA in real devices, the series resistance got from four-probe method was divided by a factor by assuming the series resistance has a liner relationship with the PTAA thickness. As shown in Figure 3, the resistivity variation measured by four-probe method follows the same trend with that derived from J-V curves, confirming F4-TCNQ doping can change the PTAA resistivity. It is noted that the resistance measured by a four-probe method is slightly larger than the resistance measured by J-V slope. One possible reason is the four-probe method measures the resistivity of film in lateral direction and the resistivity of PTAA film in the lateral and
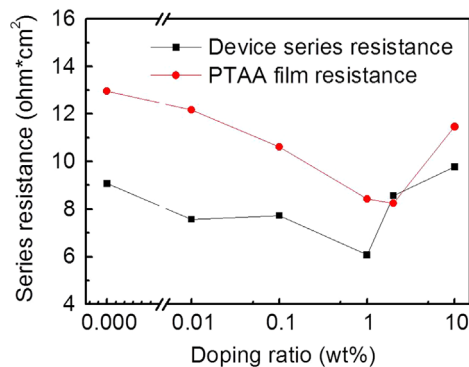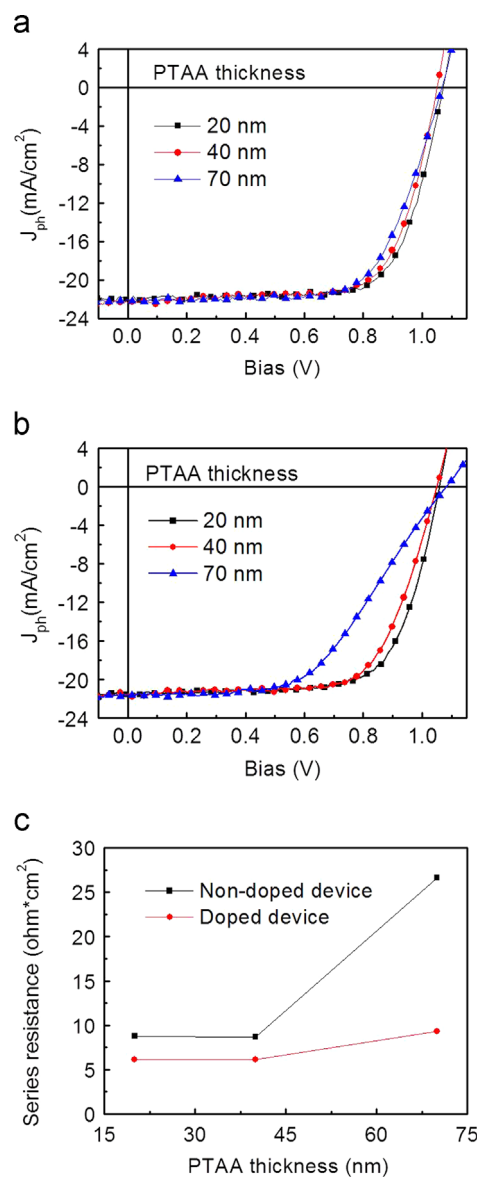
Figure 3 Series resistance of PTAA films with different F4-TCNQ doping levels. The series resistance was measured by four probe method and slope of device I–V curve.

vertical directions can be different. Another possible reason is the electric field in *J–V* measurement is much larger than that in the four-probe measurement. In addition, the thickness of PTAA layer in devices was thin and may barely cover the whole substrate.

Now that we have demonstrated the doping effect of F4-TCNQ in changing the resistivity of the PTAA layer, the influence of resistance on device efficiency needs to be clarified. Here, we applied the equivalent circuit and simulation method in inorganic solar cell to calculate *FF*s. Details about the calculation can be found in the experimental section. The two curves in Figure 2b are the device *FF*s derived and *J–V* measured. The calculated FF variation is in good agreement with the measured data, indicating series resistance variation is the primary reason for the *FF* change in our devices. The calculation also implies the importance of reducing series resistance for further device PCE enhancement. The up limit of *FF* was calculated from Eq. (4) in the experimental section to be 89%, which provides a large potential for efficiency enhancement and great promise to boost PCE exceeding 20%. Since F4-TCNQ can only change the resistivity by several times, better dopants are expected in the future study to further reducing the resistivity and increasing *FF*.

Another merit for F4-TCNQ doping is that the reduced HTL resistance should make the device efficiency less dependent on HTL thickness. To demonstrate it, we compared the devices with doped or non-doped PTAA HTLs with different HTL thicknesses from 20 nm to 70 nm. Figure 4a-b shows the *J–V* curves of devices with and without F4-TCNQ doping, respectively. Without doping, the device *J–V* curve gradually showed s-kink when the HTL thickness increased to 70 nm. On the other hand, the devices with 1 wt% F4-TCNQ doped PTAA HTLs have PCE almost insensitive to PTAA film thickness. Figure 4c summarizes the series resistance of the devices with non-doped and doped PTAA of different thicknesses. For the devices containing 20 nm HTL, 1 wt% F4-TCNQ doping reduced the series resistance from 8.8 Ω cm^2 to 6.2 Ω cm^2. Lower series resistance was observed in the doped device, especially when the HTL is thick. The resistivity of the device with 70 nm HTL was reduced three times from 26.6 Ω cm^2 to 9.33 Ω cm^2 after doping with 1 wt % F4-TCNQ. The insensitivity of device PCE on HTL thickness

Figure 4 Photocurrents of the devices with doped (a) or non-doped (b) HTL under AM 1.5 simulated illumination. The HTL thickness was varied from 20 nm to 70 nm. (c) Corresponding series resistance of the doped or non-doped HTL films derived from the slope of I–V curves.

is benefit for device reproducibility and especially attractive for large-area device fabrication.

Conclusion

In conclusion, we reported the increased device FF and enhanced device PCE of OTP solar cells using a doped polymer hole transport layer. By optimizing doping level, a high device PCE of 17.5% was achieved. This study emphasized the advantages of doping hole transport layer on the PCE of OTP solar cells and pointed out a direction of further increasing the efficiency of OTP PHJ solar cells to above 20% by exploring better dopants.

References

[1] M.M. Lee, J. Teuscher, T. Miyasaka, T.N. Murakami, H.J. Snaith, Science 338 (2012) 643–647.

[2] S.D. Stranks, G.E. Eperon, G. Grancini, C. Menelaou, M.J. Alcocer, T. Leijtens, L.M. Herz, A. Petrozza, H.J. Snaith, Science 342 (2013) 341–344.

[3] Q. Dong, Y. Fang, Y. Shao, P. Mulligan, J. Qiu, L. Cao, J. Huang, Science 347 (2015) 967–970.

[4] G. Xing, N. Mathews, S. Sun, S.S. Lim, Y.M. Lam, M. Grätzel, S. Mhaisalkar, T.C. Sum, Science 342 (2013) 344–347.

[5] D. Shi, V. Adinolfi, R. Comin, M. Yuan, E. Alarousu, A. Buin, Y. Chen, S. Hoogland, A. Rothenberger, K. Katsiev, Science 347 (2015) 519–522.

[6] W.J. Yin, T. Shi, Y. Yan, Adv. Mater. 26 (2014) 4653.

[7] W.-J. Yin, T. Shi, Y. Yan, Appl. Phys. Lett. 104 (2014) 063903.

[8] N.J. Jeon, J. Lee, J.H. Noh, M.K. Nazeeruddin, M. Grätzel S.I. Seok, J. Am. Chem. Soc. 35 (2013) 19087–19090.

[9] P. Qin, S. Paek, M.I. Dar, N. Pellet, J. Ko, M. Grätzel M.K. Nazeeruddin, J. Am. Chem. Soc. 136 (2014) 8516.

[10] J.H. Kim, P.W. Liang, S.T. Williams, N. Cho, C.C. Chueh M.S. Glaz, D.S. Ginger, A.K.Y. Jen, Adv. Mater. 27 (2014) 695.

[11] J. Liu, Y. Wu, C. Qin, X. Yang, T. Yasuda, A. Islam, K. Zhang, W. Peng, W. Chen, L. Han, Energy Environ. Sci. 7 (2014) 2963–2967.

[12] J.A. Christians, R.C. Fung, P.V. Kamat, J. Am. Chem. Soc. 136 (2013) 758–764.

[13] Q. Wang, Y. Shao, Q. Dong, Z. Xiao, Y. Yuan, J. Huang, Energy Environ. Sci. 7 (2014) 2359–2365.

[14] Z. Xiao, C. Bi, Y. Shao, Q. Dong, Q. Wang, Y. Yuan, C. Wang, Y. Gao, J. Huang, Energy Environ. Sci. 7 (2014) 2619–2623.

[15] W. Nie, H. Tsai, R. Asadpour, J.-C. Blancon, A.J. Neukirch, G. Gupta, J.J. Crochet, M. Chhowalla, S. Tretiak, M.A. Alam, H.-L. Wang, A.D. Mohite, Science 347 (2015) 522–525.

[16] Z. Xiao, Q. Dong, C. Bi, Y. Shao, Y. Yuan, J. Huang, Adv. Mater. 26 (2014) 6503–6509.

[17] J.M. Ball, M.M. Lee, A. Hey, H.J. Snaith, Energy Environ. Sci. 6 (2013) 1739–1743.

[18] J.-H. Im, I.-H. Jang, N. Pellet, M. Grätzel, N.-G. Park, Nat. Nanotechnol. 9 (2014) 927–932.

[19] D. Zhao, M. Sexton, H.Y. Park, G. Baure, J.C. Nino, F. So, Adv. Energy Mater. 5 (2015) 1401855.

[20] O. Malinkiewicz, C. Roldol-Carmona, A. Soriano, E. Bandiello, L. Camacho, M.K. Nazeeruddin, H.J. Bolink, Adv. Energy Mater. 4 (2014) 1400345.

[21] Q. Wang, Y. Shao, H. Xie, L. Lyu, X. Liu, Y. Gao, J. Huang, Appl. Phys. Lett. 105 (2014) 163508.

[22] N. Koide, A. Islam, Y. Chiba, L. Han, J. Photochem. Photobiol. A: Chem. 182 (2006) 296–305.

[23] R. Dong, Y. Fang, J. Chae, J. Dai, Z. Xiao, Q. Dong, Y. Yuan, A. Centrone, X.C. Zeng, J. Huang, Adv. Mater. (2015). http://dx.doi.org/10.1002/adma.201405116.

[24] C. Bi, Y. Shao, Y. Yuan, Z. Xiao, C. Wang, Y. Gao, J. Huang J. Mater. Chem. A 2 (2014) 18508–18514.

[25] C. Bi, Q. Dong, Y. Shao, Q. Wang, Y. Yuan, Z. Xiao, J. Huang, Nat. Commun., submitted (2015).

[26] Y. Shao, Z. Xiao, C. Bi, Y. Yuan, J. Huang, Nat. Commun. 5 (2014) 5784.

[27] D.T. Duong, H. Phan, D. Hanifi, P.S. Jo, T.Q. Nguyen, A. Salleo, Adv. Mater. 26 (2014) 6069–6073.

[28] F. Deschler, D. Riedel, A. Deák, B. Ecker, E. von Hauff, E. Da Como, Synth. Met. 199 (2015) 381–387.

[29] X. Han, Z. Wu, B. Sun, Org. Electron. 14 (2013) 1116–1121.

[30] P. Pingel, L. Zhu, K.S. Park, J.r.-O. Vogel, S. Janietz, E.-G. Kim, J.r.P. Rabe, J.-L. Brédas, N. Koch, J. Phys. Chem. Lett. 1 (2010) 2037–2041.

Qi Wang received his B.S. in 2010 and M.S. in 2013 from University of Electronic Science and Technology of China. Thereafter, he joined Dr. Jinsong Huang's research group in the Department of Mechanical and Materials Engineering at the University of Nebraska-Lincoln as a PhD student. His current research interests include device engineering and device physics of perovskite solar cell.

Cheng Bi received his BS and MS degree from Donghua University in 2007 and 2010, respectively. He is now a PhD candidate in University of Nebraska-Lincoln. His research interests include device engineering of perovskite solar cell.
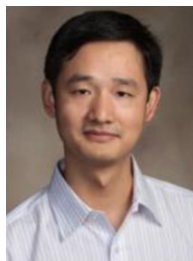
Jinsong Huang received his PhD degree in Material Science and Engineering from the University of California-Los Angeles in 2007. He is now Susan J. Rosowski Associate Professor in the Department of Mechanical Engineering at University of Nebraska-Lincoln (UNL). His current research interests include solution processed electronic materials for applications in sensing, energy and consumer electronics.